

# The *BeppoSAX* High Energy Large Area Survey (HELLAS) - VI. The radio properties

P. Ciliegi<sup>1</sup>, C. Vignali<sup>2</sup>, A. Comastri<sup>1</sup>, F. Fiore<sup>3</sup>, F. La Franca<sup>4</sup> and G.C. Perola<sup>4</sup>

<sup>1</sup> *INAF - Osservatorio Astronomico di Bologna, Via Ranzani 1, I-40127 Bologna, Italy*

<sup>2</sup> *Department of Astronomy and Astrophysics, The Pennsylvania State University, 525 Davey Lab, University Park, PA 16802, USA*

<sup>3</sup> *INAF - Osservatorio Astronomico di Roma, Via Frascati 33, I-00040, Monteporzio Catone, Italy*

<sup>4</sup> *Dipartimento di Fisica, Università di Roma Tre, Via della Vasca Navale 84, I-00146 Roma, Italy*

29 September 2018

## ABSTRACT

We present results of a complete radio follow-up obtained with the VLA and ATCA radio telescopes down to a 6 cm flux limit of about 0.3 mJy ( $3\sigma$ ) of all the 147 X-ray sources detected in the *BeppoSAX* HELLAS survey. We found 53 X-ray/radio likely associations, corresponding to about one third of the X-ray sample. Using the two point spectral index  $\alpha_{ro}=0.35$  we divided all the HELLAS X-ray sources in radio quiet and radio loud. We have 26 sources classified as radio-loud objects, corresponding to  $\sim 18\%$  of the HELLAS sample. In agreement with previous results, the identified radio-loud sources are associated mainly with Type 1 AGNs with  $L_{5-10\text{ keV}} \gtrsim 10^{44}$  erg/s, while all the identified Type 2 AGNs and Emission Line Galaxies are radio quiet objects with  $L_{5-10\text{ keV}} \lesssim 10^{44}$  erg/s. The analysis of the radio spectral index suggests that Type 1 AGNs have a mean radio spectral index ( $\langle \alpha_{AGN1} \rangle = 0.25 \pm 0.1$ ) flatter than Type 2 AGNs and Emission Line Galaxies ( $\langle \alpha_{AGN2} \rangle = 0.69 \pm 0.11$ ). This result is in agreement with the idea that the core-dominated radio emission from Type 1 AGNs is self-absorbed, while in AGN2 and Emission Line Galaxies the radio emission take place on larger physical scale, without self-absorption.

**Key words:** Surveys – radio continuum: galaxies – quasar : general

## 1 INTRODUCTION

Radio follow-up of X-ray sources have played an important role in the optical identification program of the X-ray sources by providing position accurate to  $\sim 1''$ . This was particular true for the X-ray sources detected during the *Einstein*, *ASCA* and *BeppoSAX* X-ray missions for which the typical positional error is a circle of about 1 arcmin radius. A radio detection within the X-ray error box gives fundamental information on the position of the X-ray sources. In fact, since the majority of the bright extragalactic X-ray sources are associated with AGN, a radio source within the X-ray error box is physically associated to the X-ray source with a very high probability. For this reason, many of the optical identification programs of the X-ray sources have made an intensive use of the radio data (see for example Stocke et al. 1991 for the identification of the X-ray sources of the *Einstein* Extended Medium Sensitivity Survey (EMSS) and Akiyama et al. 2000 for the identification of the X-ray sources in the *ASCA* Large Sky Survey (LSS)).

Moreover, the radio data coupled with the optical and

X-ray photometry allow us to compute the broad-band two point spectral indices  $\alpha_{ro}$  and  $\alpha_{ox}$  providing valuable information on the nature of the X-ray source population even in the absence of optical spectroscopy (Stocke et al. 1991).

A complete radio follow-up of X-ray selected samples is also an important tool to study the differences between AGNs that are strong radio-sources (radio-loud, RL) and those that are radio-quiet (RQ). Although the two classes have similar spectral index distributions (SEDs) outside the radio band (Elvis et al. 1994), their luminosity functions show differences in all the bands in which they have been studied (La Franca et al. 1994). In the optical band, using the PG sample of optically selected AGN, Padovani (1993) has shown that the shapes of the luminosity functions for RL and RQ are different. Similar results have been obtained by Della Ceca et al. 1994 and Ciliegi et al. 1995 studying the X-ray luminosity function (XLF) of RL and RQ separately. In particular Della Ceca et al. (1994) found a flattening of the XLF of the RL sample for  $L_x \leq 10^{44.5}$  erg s<sup>-1</sup>. As a result the expected fraction of RL AGNs is a function of

the X-ray flux limit in X-ray surveys. They predict that this fraction is  $\sim 13$  per cent for  $f_x(0.3 - 3.5 \text{ keV}) \sim 2 \times 10^{-13} \text{ erg cm}^{-2} \text{ s}^{-1}$  and decreases to  $\sim 2.5$  per cent for  $f_x(0.3 - 3.5 \text{ keV}) \sim 2 \times 10^{-15} \text{ erg cm}^{-2} \text{ s}^{-1}$ .

Radio follow-ups of X-ray selected samples seems to confirm this prediction. In fact, while shallow X-ray sample like the *ASCA* Large Sky Survey (Akiyama et al. 2000) with a flux limit of  $f_x(2 - 10 \text{ keV}) \sim 1 \times 10^{-13} \text{ erg cm}^{-2} \text{ s}^{-1}$  shows a fraction of RL around 10 per cent, deep ( $f_x(0.5 - 2.0 \text{ keV}) \simeq 5 - 10 \times 10^{-15} \text{ erg cm}^{-2} \text{ s}^{-1}$ ) ROSAT samples show a fraction of RL between 2 and 4 per cent (Ciliegi et al. 1995, de Ruiter et al. 1997, Zamorani et al. 1999).

In this paper we report the results of the radio follow-up of all the 147 X-ray sources detected by the *BeppoSAX*-MECS instrument in the framework of the High Energy LLarge Area Survey (HELLAS). This survey has observed about  $85 \text{ deg}^2$  of the sky in the 5-10 keV band down to a flux of  $4.5 \times 10^{-14} \text{ erg cm}^{-2} \text{ s}^{-1}$ . The whole survey and catalogue is described by Fiore et al. (2001), while the synthesis models for the X-ray background and the correlation with the soft X-rays have been investigated by Comastri et al. (2001) and Vignali et al. (2001). Finally, the spectroscopic identification of the HELLAS sources and the study of their evolution have been presented by La Franca et al. (2002, hereafter LF02).

## 2 RADIO OBSERVATIONS

The 20 HELLAS sources with a declination further south than  $-40 \text{ deg}$  have been observed with the Australia Telescope Compact Array (ATCA) while the 127 sources with  $\text{DEC} > -40 \text{ deg}$  have been observed with the Very Large Array (VLA). For these latter sources a complete covering at 20 cm down to the  $5 \sigma$  flux limit of 2.5 mJy is already available with the NRAO/VLA Sky Survey (NVSS, Condon et al. 1998) while the FIRST survey (Faint Images of the Radio Sky at Twenty centimeters, White et al. 1997) is available only for 27 HELLAS sources ( $5 \sigma$  limit of  $\sim 1 \text{ mJy}$ ).

In order to obtain information also on the radio spectral properties of the HELLAS sources we adopted the following strategy. All the 147 HELLAS sources have been observed at 6 cm down to a  $1 \sigma$  flux limit of  $\sim 0.10\text{--}0.25 \text{ mJy}$ . For the 20 HELLAS sources observed with the ATCA, we take advantage of the fact that the 6 and 3 cm receivers of the ATCA share a common feed-horn and we observed simultaneously also at 3 cm, obtaining a 3cm flux limit of  $\sim 0.22 \text{ mJy}$  ( $1 \sigma$  level).

The wavelength of 6 cm and the flux limit reached ( $0.10\text{--}0.25 \text{ mJy}$ ) can be considered a good compromise between a deep radio survey and the necessity of avoiding strong contamination from spurious radio sources within the X-ray error box. The expected number of 6 cm sources is in fact  $N(S) = (0.42 \pm 0.05)(S/30)^{-1.18 \pm 0.19}$  where  $N(S)$  is the number of sources per  $\text{arcmin}^2$  with a flux density  $> S \mu\text{Jy}$  (Fomalont et al. 1991). Considering for the X-ray error box a circle of 1 arcmin radius (see below) and a  $3 \sigma$  limit of 0.3 mJy, we expect that only 0.1 radio source lies just by chance within the HELLAS error box. Going deeper in the radio flux (reaching, for example, a  $3 \sigma$  limit of 0.05 mJy) will increase the number of chance coincidence within the

HELLAS error box to 0.7. On the other hand, at 20 cm the situation is more critical, since at 0.3 mJy the number of chance coincidence expected within an HELLAS error box is  $\sim 0.3$ .

### 2.1 The ATCA observations

The ATCA observations of the 20 HELLAS sources were performed on June 1999. They were made with the ATCA simultaneously at two different frequencies: 4.848 and 8.640 GHz (referred to as 6 and 3 cm in the rest of the paper). The synthesized beam (full width at half power) is 2 arcsec at 6 cm and 1 arcsec at 3 cm. The primary flux density calibrator was PKS B1934–638, whose flux densities at different frequencies are incorporated directly in the calibration software. The data were calibrated and reduced using the ATCA reduction package MIRIAD (Multi-channel Image Reconstruction Image Analysis and Display). For each field a  $512 \times 512$  pixel image was constructed, with a pixel size of 1 arcsec at 6 cm and of 0.3 arcsec at 3 cm. The minimum root mean square (rms) noise obtained in each field is  $\sim 0.25 \text{ mJy}$  at 6 cm and  $\sim 0.22 \text{ mJy}$  at 3 cm ( $1 \sigma$  level).

### 2.2 The VLA observations

The VLA observations were performed on 11 April 2000 at 4.885 GHz (6 cm) in C configuration. With this configuration and frequency, the synthesized beam size is  $\sim 4 \text{ arcsec}$ . All the data were analyzed with the NRAO AIPS reduction package. The data were calibrated using 3C286 as primary flux density calibrator. As for the ATCA data, for each field a  $512 \times 512$  pixel image ( $\sim 8.5 \times 8.5 \text{ arcmin}^2$ ) was constructed with a pixel size of 1 arcsec. For the majority of the fields the  $1 \sigma$  noise obtained in the central area is comparable to the expected one ( $\sim 0.1 \text{ mJy}$ ). There are however some fields in which the noise is slightly higher due to problems during data acquisitions or due to the presence of a nearby strong radio source.

## 3 X-RAY/RADIO ASSOCIATIONS

Using our 6 cm maps, we searched for radio sources within the X-ray error box of all the 147 HELLAS sources published in Fiore et al. 2001. The HELLAS error box has been assumed to be of 90 arcsec, in order to be absolutely conservative in the cross-correlation process, even though it must be noted that on average the *BeppoSAX* position of the HELLAS sources are better defined than 90 arcsec (see Appendix I of Fiore et al. 2001 for a detailed discussion of the position accuracy of the HELLAS sources). For the low number of high-Galactic latitude fields with neither a target nor a known X-ray source in the same field of view the error box has been assumed to be of 2 arcmin since no correction to the astrometry was possible (Vignali 2001).

For all the radio sources detected within the HELLAS error box we have computed the probability of random association with the X-ray source. Assuming that the radio sources belong to a Poissonian distributed population of sources,

$$P_{XR} = 1 - e^{-N(S)\pi d^2}$$

gives the probability to have a random association within a

distance  $d$  (distance between the X-ray position and the radio position of the possible counterpart) with a radio source having a flux greater than  $S$ .  $N(S)$  is the expected number of source with flux greater than that of the possible counterpart (see Section 2).

As first step,  $P_{XR} < 0.01$  was chosen as a convenient threshold to accept a radio/X-ray association. We have 32 radio/X-ray associations with  $P_{XR} < 0.01$ . However, we note that this threshold represents only a starting point in the radio X-ray association process since further and more tightening constraints on the most likely associations come from the position of the optical counterparts of the *HELLAS* sources reported in LF02. Using a subsample of 118 *HELLAS* sources (enclosed in a region with  $DEC < 79$  deg and outside  $5^h < RA < 6.5^h$  and  $17^h < RA < 20^h$ ) they report the optical identification of 61 *HELLAS* : 37 Type 1 AGN, 9 Type 2 AGN, 5 narrow emission-line galaxies (ELG), 6 Cluster, 2 BL Lac, 1 Radio Galaxy and 1 Star. Of these 61 sources, 24 have a radio counterpart within 5 arcsec and with  $P_{RO} < 0.0002$  ( $P_{RO}$  has been calculated as  $P_{XR}$  using the distance between the radio and optical position as value for  $d$ ). Assuming that all the 24 radio/optical associations are real associations (as suggested by their low  $P_{RO}$  values), we analyzed their  $P_{XR}$  values. For 19 radio/optical associations we found  $P_{XR} < 0.01$ , 4 have  $0.01 < P_{XR} < 0.1$  and one has  $P_{XR} = 0.217$ . The large value of  $P_{XR}$  for the 5 sources with  $P_{XR} > 0.01$  is due to the fact that for these sources the distance between the radio/optical position and the X-ray position is greater than 60 arcsec (see LF02 for a discussion on the procedure of the optical identification of the *HELLAS* sources). In the light of these results, we increase our threshold for the radio X-ray associations to  $P_{XR} = 0.1$  (*i.e.* we expect that about 10 per cent of the proposed identifications may be spurious positional coincidences). With this new threshold we found 53 X-ray/radio associations. We do not have X-ray sources with two (or more) radio counterparts both with  $P_{XR} < 0.1$ .

### 3.1 Optical counterparts of the X-ray/radio associations

Starting from the radio position of the 53 X-ray/radio associations, we searched for optical counterparts within 5 arcsec from the radio position using the optical positions of the 61 *HELLAS* sources identified by LF02, the USNO-A2.0<sup>1</sup> optical catalogue, the APM<sup>2</sup> optical catalogue and the Nasa Extragalactic Database (NED). As said above, 24 X-ray/radio associations have been identified with sources in LF02 (10 Type 1 AGN, 4 Type 2 AGN, 2 BL LAC, 3 Clusters, 4 ELGs and 1 Radio galaxy), 1 has been identified with a  $z=0.708$  Radio galaxy in the Lockman Hole using NED (see table 2 source 116 in Lehmann et al. 2000 for a description of this source), 13 have an optical (R band) identification in the USNO and/or APM catalogue while 15 X-ray/radio associations do not have an optical identification brighter than  $R=20$ . The list of all the 147 *HELLAS* sources with their most probable optical and radio counterparts is shown in Table 1. The first three columns show the X-ray position,

the offset in arcmin in the *BeppoSAX* field and the 5-10 keV X-ray flux in units of  $10^{-13}$  erg cm<sup>-2</sup> s<sup>-1</sup> (from Fiore et al. 2001). Columns IV, V and VI give the R band magnitude (from LF02 if not otherwise specified), spectroscopic identification (1 for Type I AGN, 2 for Type II AGN, 3 for BL LAC, 4 for Cluster, 5 for ELG and 6 for Radio galaxies) and redshift from LF02. Columns VII, VIII, and IX give the radio flux at 3cm, 6 cm and 20 cm, respectively. All the 20 cm data are from the NVSS catalogue version 2.17 if not otherwise specified. For the X-ray sources without radio counterparts, we report at 3 and 6 cm the  $3\sigma$  upper limit of our maps while at 20 cm we report the limit of the radio catalogue used (NVSS or FIRST). Column X gives the radio spectral index calculated using the available frequencies (mainly 6 and 20 cm). Column XI gives the position of the radio sources obtained from our 6 cm map (except when the source is detected only at 20 cm). The typical positional error of 6 cm sources is below 1 arcsec. Columns XII and XIII give the distance between the radio and the X-ray position and the probability  $P_{XR}$  of a random association. Columns XIV and XV give the distance between the radio and the optical position and the probability  $P_{RO}$  of a random association. Finally columns XVI and XVII give the two point spectral indices  $\alpha_{ro}$  and  $\alpha_{ox}$  defined as  $\alpha_{ro} = \log(F_{5GHz}/F_{2500})/5.38$  and  $\alpha_{ox} = \log(F_{2500}/F_{2keV})/2.605$  where  $F_{5GHz}$  is the radio flux at 6 cm obtained from the present observation or by extrapolating the 20 cm flux density with a power-law slope with  $\alpha_r=0.7$ ,  $F_{2500}$  is the optical flux at 2500Å derived from the R magnitude with an optical slope of  $\alpha_o=0.5$  while  $F_{2keV}$  is the monochromatic X-ray flux at 2 keV derived from the measured *BeppoSAX* 5-10 keV flux and assuming an energy spectral index  $\alpha_x=0.6$  (Fiore et al. 2001).

#### 3.1.1 Comparison with the optical identification reported in LF02

As said above, 24 of the 61 sources with an optical identification reported in LF02 have a radio counterpart within 5 arcsec. In addition to this information, it is interesting to note that no other radio sources have been found within their X-ray error box, as well as no radio sources have been detected in the X-ray error box of the remaining 37 sources. Moreover, among the 13 X-ray sources classified as empty fields down to  $R=21$  in LF02, only two (0134–3006 and 1304–0533) have a radio counterpart (see Table 1). These two radio sources have not an optical identification brighter than  $R=21$  within 5 arcsec from their radio position, in agreement with their classification as empty field.

These results, under the hypothesis that a radio source within the X-ray error box is physically associated to the X-ray source with a very high probability, strengthen the goodness of the optical identification reported in LF02.

### 3.2 Radio-Loud and Radio-Quiet Classification

The two point spectral index  $\alpha_{ro}$  has been commonly used to discriminate between radio-loud and radio-quiet objects. We were able to calculate the  $\alpha_{ro}$  value for a total of 84 sources: 55 *HELLAS* sources identified in LF02 (we did not calculate the two point spectral indices for the 6 clusters due to the indetermination of their optical magnitude), for

<sup>1</sup> <http://archive.eso.org/skycat/servers/usnoa>

<sup>2</sup> <http://www.ast.cam.ac.uk/~apmcat/>

<i>BeppoSAX</i> Position RA(2000) DEC(2000)	Offx ( $''$ )	Fx	R	ID	z	F8.6 (mJy)	F5 (mJy)	F1.4 (mJy)	$\alpha_r$	Radio Position RA(2000) DEC(2000)	$\Delta_{XR}$ ( $''$ )	$P_{XR_2}$ $\times 10^{-2}$	$\Delta_{RO}$ ( $''$ )	$P_{RQ}$ $\times 10^{-6}$	$\alpha_{ro}$	$\alpha_{ox}$
00 26 36.5 −19 44 13	13.2	3.39	18.1	2	0.238		<0.30	<2.5							<0.09	1.23
00 27 09.9 −19 26 19	6.2	1.83	17.7	1	0.227		<0.30	<2.5							<0.06	1.40
00 27 43.9 −19 30 29	11.0	1.58					<0.30	<2.5								
00 45 49.6 −25 15 13	23.7	3.26	17.5	2	0.111		<0.30	<2.5							<0.05	1.33
00 48 05.8 −25 04 32	14.9	1.48					<0.40	<2.5								
01 18 03.9 +89 20 12	8.3	0.87					<0.30	<2.5								
01 21 56.8 −58 44 05	15.6	2.57	16.8	2	0.118	<0.65	<0.75	<2.5							<0.07	1.48
01 34 14.3 −29 45 41	14.2	1.50					<0.35	<2.5								
01 34 28.6 −30 06 34	12.2	1.33	>20				0.41±0.05	4.3±0.5	1.89	01 34 25.61 −30 05 50.90	57.9	5.46			>0.26	<1.10
01 34 33.3 −29 58 38	6.0	0.87	18.0	1	2.217		<0.35	<2.5							<0.10	1.48
01 34 49.6 −30 02 34	5.4	0.71					<0.35	<2.5								
01 35 30.2 −29 51 21	8.4	0.90	17.7	1	1.344		<0.35	<2.5							<0.07	1.52
01 40 08.9 −67 48 13	8.0	2.83	12.4	0	0.000	<0.65	<0.75	<2.5							<−0.26	2.14
01 53 03.9 +89 12 20	2.4	0.54					<0.35	<2.5								
02 42 01.8 +00 00 46	10.0	1.47	18.6	1	1.112		<0.45	<2.5							<0.16	1.30
02 42 09.4 +00 02 29	7.5	0.68	18.4 <sup>u</sup>				1.65±0.20	<2.5	<0.33	02 42 14.53 +00 02 51.95	80.3	2.07	1.1	3.71	0.25	1.46
03 08 08.5 +89 08 41	4.9	0.65					<0.30	<2.5								
03 08 19.0 +02 46 27	18.5	5.09	>20					7.4±0.5		03 08 21.80 +02 46 34.50	42.6	0.29			>0.33	<0.88
03 15 45.0 −55 29 26	14.5	2.65	17.9	1	0.464	<0.65	<0.75	<2.5							<0.15	1.31
03 17 32.4 −55 20 12	21.0	4.10	17.5	1	0.406	<0.65	<0.75	<2.5							<0.12	1.30
03 33 09.6 −36 19 40	15.2	3.98	17.5	3	0.308			13.6±0.6		03 33 12.54 −36 19 47.51	36.3	0.10	4.1	9.90	0.28	1.30
03 34 07.4 −36 04 22	5.1	1.95	20.1	1	0.904		<2.5	<2.5							<0.30	1.02
03 36 51.3 −36 15 57	14.7	3.72	17.7	1	1.537		583±42	501±15	-0.12	03 36 54.01 −36 16 05.11	33.7	0.00	0.9	0.00	0.67	1.28
04 32 27.9 +05 13 05	15.0	2.06					<0.75	<2.5								
04 37 14.5 −47 30 58	16.0	2.68	17.3	1	0.142	<0.65	<0.75	<2.5							<0.11	1.40
04 38 47.9 −47 29 06	20.1	4.69	20.5	1	1.453	94.99±1.5	132.3±2.2	<2.5	0.58	04 38 47.01 −47 28 00.91	65.7	0.01	1.1	0.02	0.73	0.81
05 02 15.5 +12 04 07	20.9	7.41	>20				<0.30	<2.5								
05 15 13.7 +01 08 07	7.6	1.26	>20				0.48±0.05	<2.5	<1.33	05 15 11.83 +01 08 20.98	31.3	1.35			>0.27	<1.11
05 20 48.3 −45 42 00	9.6	5.90	>20			<0.65	4.90±0.10	<2.5		05 20 44.78 −45 41 27.33	49.3	0.22			>0.46	<0.85
05 48 41.3 −60 52 18	19.5	2.42				<0.65	<0.75	<2.5								
05 50 00.2 −61 02 22	5.9	0.90	14.5 <sup>u</sup>			<0.65	0.97±0.10	<2.5	>0.70	05 50 06.61 −61 01 23.26	75.0	3.35	2.6	40.99	−0.08	2.01
05 52 06.1 −60 59 48	11.1	1.23				<0.65	<0.75	<2.5								
05 52 51.3 −60 57 18	17.1	2.06				<0.65	<0.75	<2.5								
06 23 56.6 −69 21 13	6.1	1.33	17.4 <sup>u</sup>			<0.65	0.59±0.10	<2.5	>−0.17	06 23 50.91 −69 20 08.07	71.5	5.42	0.5	2.72	0.09	1.50
06 25 31.3 −69 19 09	6.4	1.42				<0.65	<0.75	<2.5								
06 46 39.3 −44 15 35	16.6	4.27	16.6	1	0.153		<0.50	<2.5							<0.02	1.43
06 46 42.7 −44 32 29	19.0	2.68					<0.50	<2.5								
06 55 39.6 +79 10 48	4.6	0.75					<0.30	<2.5								
07 21 29.6 +71 14 04	8.1	0.84	17.7	1	0.232		<0.40	<2.5							<0.08	1.53
07 41 40.3 +74 14 57	22.6	30.66	...	4	0.216		1.50±0.15	22.7±1.6	2.19	07 41 44.70 +74 14 39.76	24.9	0.22	2.0	14.50		
07 41 45.2 +74 26 23	13.1	3.74					<0.35	<2.5								
07 43 09.1 +74 29 19	7.2	6.05	16.4	1	0.312		<0.35	<2.5							<−0.02	1.40
08 37 37.2 +25 47 48	12.1	2.63	16.9	1	0.077		1.07±0.10	1.18±0.15	0.09	08 37 37.03 +25 47 50.47	3.4	0.00	1.8	17.50	0.10	1.46
08 38 59.9 +26 08 13	23.0	16.38	15.3	5	0.048		1.89±0.15	5.19±0.15	0.81	08 38 59.27 +26 08 13.07	8.5	0.02	1.3	4.66	0.03	1.40
09 46 05.3 −14 02 59	15.8	2.82					<0.35	<2.5								
09 46 17.9 −14 10 27	10.9	2.04	18.7 <sup>a</sup>				0.37±0.05	<2.5	<1.54	09 46 21.89 −14 10 50.29	62.5	7.12	3.0	170.16	0.15	1.23
09 46 32.8 −14 06 15	16.4	3.22					<0.30	<2.5								
10 29 19.1 +50 48 15	17.5	5.78					<0.35	<1.0								
10 32 15.8 +50 51 03	10.4	3.13	15.9	1	0.174		<0.30	<1.0							<−0.07	1.59
10 34 43.1 +39 29 18	8.4	1.11					<0.30	<1.0								
10 34 52.0 +39 40 12	5.3	1.41	16.5 <sup>u</sup>				<0.30	<1.0	>1.30	10 34 56.41 +39 39 40.78	59.8	3.61	0.5	1.46	−0.03	1.63
10 52 45.4 +57 30 42	4.0	0.83	20.9 <sup>l</sup>	6 <sup>l</sup>	0.708 <sup>l</sup>		16.09±0.15	65.0±2.30	1.12	10 52 37.39 +57 31 04.09	68.2	0.10	0.0	0.00	0.62	1.04
10 54 19.8 +57 25 09	13.4	2.62	18.5	2	0.205		0.50±0.05	1.44±0.15	0.83	10 54 21.14 +57 25 44.63	37.2	1.81	0.8	8.48	0.16	1.22
10 54 21.7 +57 36 24	16.6	2.13	17.6 <sup>u</sup>				37.30±0.15	191.4±6.70	1.32	10 54 26.24 +57 36 48.19	43.8	0.02	1.2	0.12	0.44	1.39
11 01 46.4 +72 26 11	22.3	7.29	16.7	1	1.460		864.1±1.30	1245.0±37.4	0.29	11 01 48.92 +72 25 38.00	34.9	0.00	0.5	0.00	0.63	1.32
11 02 37.2 +72 46 38	20.7	7.87	15.1	1	0.089		<0.30	<2.5							<−0.13	1.56
11 06 14.0 +72 43 16	8.5	1.67	18.5	1	0.680		<0.30	<2.5							<0.12	1.29
11 07 04.9 −18 16 28	7.7	1.23					<0.30	<2.5								
11 18 11.9 +40 28 33	4.2	0.85	18.7	1	0.387		<0.35	<1.0							<0.15	1.37
11 18 46.2 +40 27 39	4.8	1.39	18.5	1	1.129		<0.30	<1.0							<0.12	1.32
11 34 52.7 +70 23 09	15.5	3.77					<0.30	<2.5								
11 56 39.2 +65 17 57	5.7	0.75					<0.30	<2.5								
11 57 01.7 +65 27 24	15.4	2.14					<0.30	<2.5								
12 04 07.6 +28 08 30	16.1	5.10		4	0.167		<0.30	<1.0								
12 17 45.1 +47 29 55	16.4	3.24	>20				0.41±0.07	<1.0	<0.72	12 17 51.07 +47 30 13.58	63.3	6.49			>0.26	<0.95
12 17 50.3 +30 07 08	19.8	3.54	14.0	3	0.237		384.8±3.1	571.6±21.4	0.32	12 17 52.08 +30 07 00.33	24.3	0.00	1.7	0.02	0.36	1.86
12 18 55.0 +29 58 12	12.7	1.98	18.6	2	0.176		<0.30	<1.0							<0.13	1.25
12 19 21.6 +47 11 07	9.4	1.32	>20				<0.30	9.08±0.15	>2.75	12 19 21.27 +47 12 13.46	66.5	0.69			>0.23	<1.10
12 19 45.7 +47 20 42	7.5	1.17	19.3	1	0.654		1.21±0.05	2.90±0.50	0.70	12 19 52.36 +47 20 58.65	69.7	2.24	0.9	3.78	0.29	1.23
12 22 06.8 +75 26 17	6.5	2.46	...	4	0.240		1.60±0.05	<2.5	<0.36	12 22 06.50 +75 26 14.9	2.2	0.00	0.1	0.00		
12 29 23.7 +01 51 38	14.1	1.61					<4.0	<24.5								
12 40 26.0 −05 13 20	11.7	3.13	18.8	1	0.300		<0.30	<1.0							<0.14	1.14
12 40 29.6 −05 07 46	16.8	1.92	15.2	5	0.008		<0.30	1.30±0.15	>1.18	12 40 36.89 −05 07 52.80	109.0	21.7	4.3	108.16	0.14	1.77
12 54 28.0 +59 21 01	24.3	6.37					<0.30	<2.5								
12 55 16.6 −05 39 22	16.3	2.20					<3.00	<5.6								
12 56 09.9 −05 54 30	7.6	0.91					<3.00	<5.6								

<i>BeppoSAX</i> Position RA(2000) DEC(2000)	Offx ( $''$ )	Fx	R	ID	z	F8.6 (mJy)	F5 (mJy)	F1.4 (mJy)	$\alpha_r$	Radio Position RA(2000) DEC(2000)	$\Delta_{XR}$ ( $''$ )	$P_{XR}$ $\times 10^{-2}$	$\Delta_{RO}$ ( $''$ )	$P_{RO}$ $\times 10^{-6}$	$\alpha_{ro}$	$\alpha_{ox}$
13 04 24.3 –10 23 53	4.4	1.28					<1.00	<2.5								
13 04 38.2 –10 15 47	5.9	1.43					<0.30	<2.5								
13 04 45.1 –05 33 37	7.5	1.26	20.1	1	2.386		0.58 $\pm$ 0.05	<1.5	<0.76	13 04 44.22 –05 33 40.21	13.5	0.20			<0.24	1.07
13 05 32.3 –10 32 35	22.0	19.27	14.9	1	0.278		1149.6 $\pm$ 1.0	711.3 $\pm$ 21.3	–0.39	13 05 33.02 –10 33 19.12	45.4	0.00	0.9	0.00	>0.29	<1.11
13 05 36.5 –05 43 30	22.7	6.42	>20				2.10 $\pm$ 0.11	6.30 $\pm$ 0.50	0.88	13 05 36.10 –05 42 00.31	89.7	1.94			0.52	1.44
13 36 34.3 –33 57 47	21.8	3.18	10.5	6	0.013	440 <sup>n</sup>	1886 <sup>n</sup> $\pm$ 132	2730.4 <sup>n</sup> $\pm$ 80	0.30	13 36 39.01 –33 57 58.00	60.0	0.00	0.1	0.00	>0.39	<0.84
13 38 34.1 +48 21 05	4.3	1.24					<0.30	<1.0							0.23	2.41
13 42 47.9 +00 21 09	16.9	2.48	19.8 <sup>a</sup>				29.5 $\pm$ 0.5	96.8 $\pm$ 3.5	0.96	13 42 46.03 +00 20 28.30	49.4	0.03	2.3	0.57	0.59	1.03
13 42 59.3 +00 01 38	20.6	3.25	18.7	1	0.804		<0.30	<1.0							<0.14	1.15
13 48 20.8 –30 11 06	14.4	2.18	15.3 5	2	0.128		4.68 $\pm$ 0.13	10.0 $\pm$ 0.6	0.61	13 48 19.50 –30 11 54.01	50.9	0.24	2.0	3.79	0.10	1.74
13 48 24.3 –30 25 47	14.8	3.15					<0.50	<2.5								
13 48 37.9 –30 09 11	12.3	1.59					<0.50	<2.5								
13 48 45.4 –30 29 36	14.4	5.11	17.1	1	0.330		<0.30	<2.5							<0.02	1.32
13 50 09.4 –30 19 55	10.8	5.08	16.5 4	5	0.074		0.69 $\pm$ 0.11	<2.5	<1.04	13 50 15.37 –30 20 09.58	78.6	5.44	0.6	3.26	0.04	1.41
13 53 54.6 +18 20 33	17.5	6.82	17.3	1	0.217		0.43 $\pm$ 0.05	<1.0	<0.68	13 53 54.43 +18 20 16.59	16.6	0.43	0.7	7.76	0.06	1.24
13 55 54.1 +18 13 35	19.8	6.14					<0.45	<1.0								
14 11 58.7 –03 07 02	20.7	3.93					<0.35	<1.0								
14 17 12.5 +24 59 28	12.9	0.69	19.5	1	1.057		<0.30	<1.0							<0.19	1.29
14 18 31.1 +25 11 07	8.6	6.11		4	0.240		12.8 $\pm$ 0.20	38.0 $\pm$ 1.5	0.88	14 18 32.38 +25 12 00.99	56.7	0.09	4.0	4.62		
14 38 30.1 +64 30 25	11.2	2.57	17.2 <sup>u</sup>				0.65 $\pm$ 0.05	<2.5	1.08	14 38 26.71 +64 28 59.76	88.0	7.25	0.5	0.00	0.09	1.42
14 48 21.8 –69 20 30	11.7	4.25	17.0 <sup>u</sup>			<0.65	0.95 $\pm$ 0.10	<2.5	>0.66	14 48 25.59 –69 19 52.07	42.9	1.14	2.1	27.41	0.10	1.37
15 19 39.9 +65 35 46	13.9	9.43	14.4	2	0.044		1.08 $\pm$ 0.20	<2.5	0.68	15 19 33.69 +65 36 00.80	41.2	0.90	2.8	41.88	–0.08	1.63
15 28 46.0 +19 45 10	4.7	1.65	20.3 <sup>u</sup>				1.16 $\pm$ 0.05	1.26 $\pm$ 0.16	0.09	15 28 44.59 +19 44 34.94	40.3	0.79	0.4	0.79	0.36	1.02
15 28 47.3 +19 39 10	5.0	1.57	20.3	1	0.657		<0.30	<1.0							<0.25	1.03
16 26 56.8 +55 13 24	14.2	3.15					<0.30	<1.0								
16 26 59.9 +55 28 20	10.5	12.09	...	4	0.130		<0.30	<1.0								
16 34 10.7 +59 37 44	6.9	0.50					<0.30	<2.5								
16 34 11.0 +59 48 15	5.2	0.48	17.6 <sup>u</sup>				0.87 $\pm$ 0.15	<2.5	<0.85	16 34 12.53 +59 49 13.75	59.9	2.44	1.5	15.51	0.14	1.64
16 34 11.8 +59 45 29	3.4	0.84	19.0	2	0.341		<0.30	<2.5							<0.16	1.33
16 49 57.9 +04 53 32	19.8	9.45	...	4	0.154		<0.30	<2.5								
16 50 40.1 +04 37 17	24.5	12.25	14.6	2	0.031		1.63 $\pm$ 0.10	<2.5	<0.34	16 50 42.77 +04 36 18.39	70.9	1.63	1.1	3.98	–0.03	1.56
16 52 12.5 +02 11 29	15.8	2.36					<0.30	<2.5								
16 52 38.0 +02 22 18	4.6	0.67	20.7	1	0.395		<0.30	<2.5							<0.28	1.11
16 54 41.1 +40 02 10	17.6	6.32	14.9 <sup>u</sup>				36.3 $\pm$ 0.35	80.7 $\pm$ 2.9	0.64	16 54 43.03 +40 02 46.20	42.4	0.02	2.3	0.45	0.24	1.62
17 40 10.7 +67 42 50	17.7	3.28	18.3 <sup>a</sup>				5.57 $\pm$ 0.06	4.10 $\pm$ 0.40	–0.25	17 40 22.32 +67 41 38.14	97.6	0.73	0.7	0.37	0.34	1.21
17 42 36.3 +68 00 44	10.6	2.76	>20				2.71 $\pm$ 0.09	7.3 $\pm$ 0.50	0.80	17 42 50.51 +67 59 33.50	106.5	2.02			>0.41	<0.98
17 50 25.4 +60 56 01	11.7	2.10	>20				2.11 $\pm$ 0.11	4.6 $\pm$ 0.40	0.63	17 50 38.81 +60 56 52.50	110.4	2.91			>0.39	<1.02
17 51 30.3 +61 00 43	6.7	0.55					<0.30	<2.5								
17 52 38.3 +61 05 47	3.2	0.36					<0.30	<2.5								
17 53 49.0 +60 59 52	12.7	1.10	>20				0.47 $\pm$ 0.10	<2.5	<1.35	17 53 47.71 +60 58 58.76	54.0	4.07			>0.27	<1.13
18 03 51.8 +61 10 21	2.9	0.60	>20				39.0 $\pm$ 0.50	132.0 $\pm$ 5.0	0.98	18 03 47.38 +61 09 22.20	66.9	0.03			>0.62	<1.23
18 15 17.5 +49 44 51	9.8	3.48					<0.30	<2.5								
18 18 58.6 +61 14 42	18.6	2.07	>20				2.54 $\pm$ 0.06	<2.5	<–0.01	18 18 51.06 +61 14 18.43	59.3	0.68			>0.40	<1.03
18 19 18.4 +60 56 06	3.5	1.52					<0.30	<2.5								
18 19 35.5 +60 58 46	2.1	0.49					<0.30	<2.5								
18 19 39.5 +60 53 26	3.7	0.83					<0.30	<2.5								
18 36 11.3 –65 07 20	22.8	4.44				<1.0	<1.0	<2.5								
20 42 47.6 –10 38 30	21.1	5.32	17.9	1	0.363		<0.30	<2.5							<0.08	1.19
20 44 34.8 –10 27 34	15.3	1.99	17.7	1	2.755		4.30 $\pm$ 0.17	8.8 $\pm$ 0.5	0.58	20 44 34.95 –10 28 09.09	35.2	0.13	2.5	6.54	0.28	1.39
21 22 59.2 +89 01 58	15.3	4.77	>20				19.50 $\pm$ 0.17	60.6 $\pm$ 1.9	0.91	21 21 36.16 +89 02 16.36	27.9	0.01			>0.57	<0.89
21 38 08.9 –14 33 13	7.0	2.34					<0.30	<2.5								
21 42 46.7 +89 35 30	23.5	10.47					<0.30	<2.5								
21 59 52.1 +88 54 53	17.8	6.85					<0.30	<2.5								
22 03 00.5 –32 04 18	16.5	2.83					<0.35	<2.5								
22 26 30.3 +21 11 56	13.7	3.91	17.6	1	0.260		<0.40	<2.5							<0.08	1.29
22 31 49.6 +11 32 08	15.2	1.94					<1.00	<2.5								
22 41 22.1 +29 42 41	15.6	2.98	>20				0.84 $\pm$ 0.11	<2.5	<0.88	22 41 27.56 +29 43 33.88	88.6	5.49			>0.31	<0.96
22 42 51.5 +29 35 32	7.6	1.02					<1.00	<2.5								
22 44 11.4 +29 51 14	23.1	3.95					<1.00	<2.5								
23 02 30.1 +08 37 06	17.6	2.67					<0.30	<2.5								
23 02 36.2 +08 56 42	10.1	3.17					<0.30	<2.5								
23 06 59.2 +08 48 40	4.1	1.02					<0.30	<2.5								
23 15 36.4 –59 03 40	8.3	2.03	11.2 2	5	0.044	11.01 $\pm$ 0.10	15.40 $\pm$ 0.10		0.58	23 15 46.72 –59 03 15.79	83.4	0.16	1.9	0.84	–0.10	2.38
23 16 09.8 –59 11 24	6.1	1.32				<0.65	<0.75									
23 19 22.1 –42 41 50	21.4	5.67	16.5	5	0.101	<0.65	<0.75								<0.05	1.39
23 27 28.7 +08 49 30	7.1	0.55	18.5	1	0.154		<0.35	<2.5							<0.13	1.48
23 27 37.1 +08 38 56	7.9	1.48					<0.35	<2.5								
23 29 02.4 +08 34 39	20.0	2.87	20.3 2	1	0.953		197.8 $\pm$ 0.40	172.9 $\pm$ 5.2	–0.11	23 29 05.79 +08 34 16.45	55.0	0.00	0.5	0.00	0.78	0.92
23 31 55.6 +19 38 34	17.0	3.75	18.8	1	0.475		<0.35	<2.5							<0.16	1.11
23 55 32.7 +28 35 11	7.7	1.72					<0.75	<2.5								
23 55 53.3 +28 36 05	12.0	4.17	17.9	1	0.731		286.7 $\pm$ 0.50	681.0 $\pm$ 20.4	0.70	23 55 54.1 +28 35 58.00	13.6	0.00	2.6	0.05	0.63	1.23

<sup>a</sup> magnitude from the APM catalogue<sup>l</sup> Lehmann et al (2000)<sup>n</sup> data from the NASA/IAPC Extragalactic Database (NED)<sup>u</sup> magnitude from the USNO catalogue

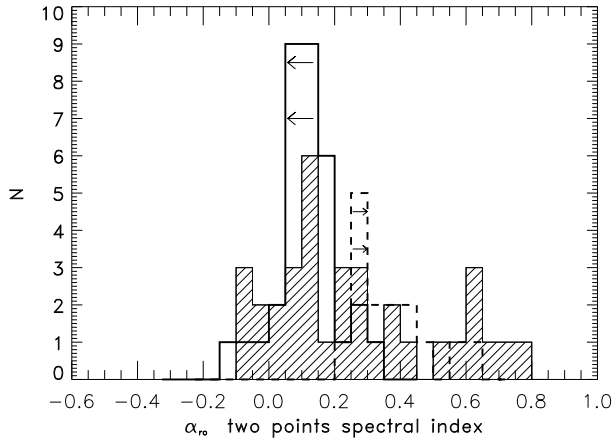


**Figure 1.** Distribution of the two point spectral index  $\alpha_{RO}$  for the HELLAS sources (sources detected both in radio and optical band: *shaded histogram*;  $3\sigma$  upper limits (X-ray sources with an optical counterpart but without a radio counterpart): *open solid line histogram*;  $3\sigma$  lower limits (X-ray sources with a radio counterpart but without an optical counterpart): *open dashed line histogram*).

the  $z=0.708$  Radio galaxy in the Lockman Hole (see above), for the 13 X-ray/radio associations that have been identified with an USNO and/or an APM source and for the 15 X-ray/radio associations without an optical counterpart (in the latter case using an optical upper limit of  $R=20$ ). The  $\alpha_{ro}$  distribution of these 84 sources is shown in Figure 1 (sources detected both in radio and optical band: *shaded histogram*;  $3\sigma$  upper limits (X-ray sources with an optical counterpart but without a radio counterpart): *open solid line histogram*;  $3\sigma$  lower limits (X-ray sources with a radio counterpart but without an optical counterpart): *open dashed line histogram*).

The values of  $\alpha_{ro}$  used in literature to discriminate between radio-loud and radio-quiet objects are 0.20 (see Elvis et al. 1994, Giommi, Menna & Padovani 1999) or 0.35 (Zamorani et al. 1981, Della Ceca et al. 1994). To choose between these two values, we applied to our  $\alpha_{ro}$  distribution (Figure 1) the Lee statistic (see Fitchett & Merriit 1988 and Lee 1979 for details). The Lee statistic is a test for a bimodality of a distribution. The location of the maximum corresponds to the value of the variable which best separates the two subsamples. The results of the Lee statistic are shown in Figure 2. We find that the Lee parameter reaches its maximum for  $\alpha_{ro} \simeq 0.35 - 0.36$ . This result has been obtained using only the distribution of the sources detected both in radio and optical band (shaded histogram in Figure 1). However similar results are obtained treating the upper and lower limits as detections. Consequently the value of  $\alpha_{ro}=0.35$  has been used to separate the RL from the RQ objects.

We have 18 RL sources with  $\alpha_{ro} \geq 0.35$  (11 have been detected both in the radio and optical bands and 7 have a lower limit on  $\alpha_{ro}$  greater than 0.35), 58 RQ sources (24 detected both in the radio and optical bands, 34 with an  $\alpha_{ro}$  upper limit lower than 0.35) while for 8 sources it was impossible to give a reliable classification due to the fact that

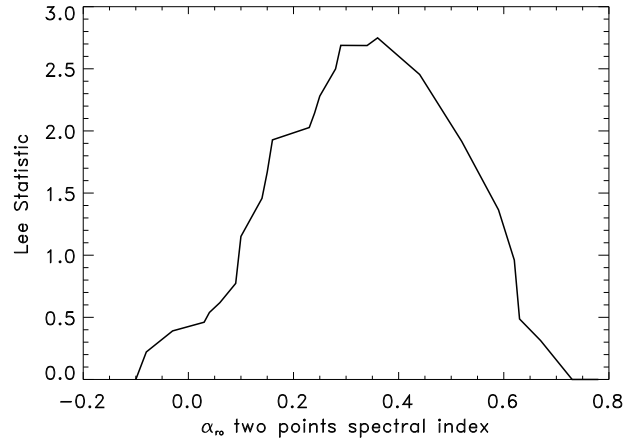


**Figure 2.** Lee statistic for the distribution of the two point spectral index  $\alpha_{ro}$ . The position of the maximum is the value of the variable which best divides the two distributions, *i.e.*, the radio-quiet and radio-loud objects.

they have an  $\alpha_{ro}$  lower limit lower than 0.35. However, given the fact that their  $\alpha_{ro}$  lower limit are close to the threshold of 0.35 (the lowest value is  $\alpha_{ro} > 0.23$ , see Table 1 and the open dashed line histogram in Figure 1) we assumed these 8 sources to be RL objects. Over 84 sources analyzed we have therefore 26 RL and 58 RQ objects. For the remaining 63 HELLAS sources it was impossible to calculate the two point spectral index  $\alpha_{ro}$  (or at least a lower or an upper limit) due to the lack of a radio and optical identification, *i.e.* for these sources only an X-ray detection and a radio upper limit is available. However also the upper limit on their radio-to-X-ray ratio can be used to obtain useful informations on the radio nature of these source. In Figure 3 (top panel) we report the distribution of the radio-to-X-ray ratio for the RQ and RL objects in the atlas of quasars published by Elvis et al. (1994) while in the the other two panels we report the distribution of the 84 HELLAS sources for which it was possible to obtain a classification as RQ and RL object (middle panel) and the distribution of the radio-to-X-ray ratio upper limits for the 63 HELLAS sources without a classification in RL and RQ (bottom panel). Although the atlas of 47 quasars from Elvis et al. (1994) is an heterogeneous sample of objects selected mainly from the PG (Schmidt and Green 1983), 3C and Parkes catalogues, it gives a useful reference for the radio-to-X-ray ratio values for RQ and RL objects. As shown in figure 3 the RQ and RL objects show a significantly different distribution of their radio-to-X-ray ratio. A Kolmogorov-Smirnov (KS) test of the radio-to-X-ray ratio distributions for the HELLAS RQ and RL (reported in the middle panel of figure 3) shows that the two distributions are drawn from the same population with a probability  $P_{KS} < 5 \times 10^{-4}$ . The same result has been obtained performing a KS test between the distribution of the RL and that of the 63 sources for which only an X-ray detection and a radio upper limit is available. Viceversa, a KS test between this latter and the distribution of the HELLAS RQ objects indicate that the hypothesis that the two distribution are drawn from the same population can not be excluded ( $P_{KS}=0.69$ ). It is therefore reasonable to assume

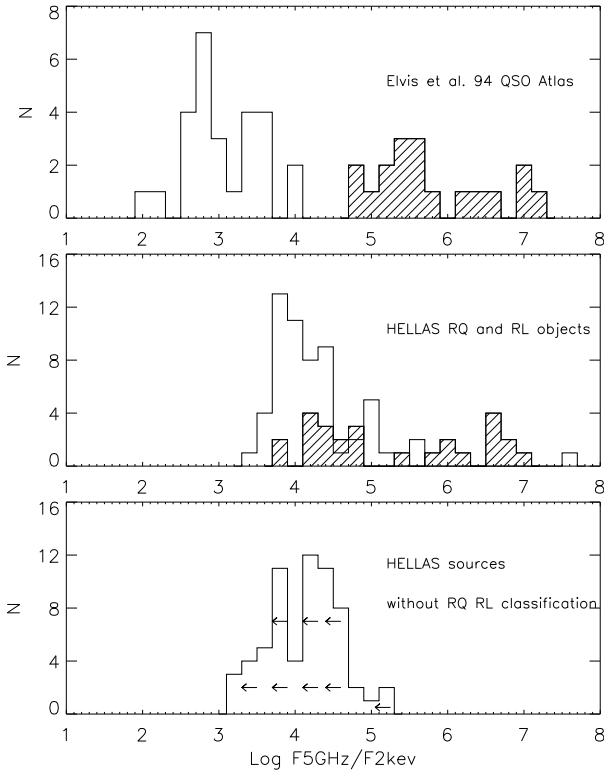


**Figure 3.** *Top panel:* radio-to-X-ray ratio distribution for the 29 Radio-Quiet (empty histogram) and 18 Radio-Loud (shaded histogram) objects in the atlas of quasars from Elvis et al. (1994). *Middle panel:* As above for the 58 Radio-Quiet and 26 Radio-Loud objects in the HELLAS survey. *Bottom Panel:* Distribution of the radio-to-X-ray ratio upper limit for the 63 HELLAS sources for which only an X-ray detection and a radio upper limit are available.

that all the 63 sources for which only an X-ray detection and a radio upper limit is available are radio-quiet objects. Under this hypothesis, the fraction of radio-loud objects in the HELLAS sample is  $\sim 18$  per cent (26 RL over a total of 147 sources).

## 4 DISCUSSION

### 4.1 Radio, Optical and X-ray properties

To examine the general properties of the radio/X-ray associations, in Figure 4 we show the 6 cm radio flux versus the R-band magnitude for the 53 radio/X-ray associations of the HELLAS sample. Superimposed are the lines corresponding to constant values for the two point spectral index  $\alpha_{ro}$ . The dot dashed line shows the value of  $\alpha_{ro}=0.35$  used to separate RL and RQ objects. In Figure 5 we plot the radio versus the hard (5-10 keV) X-ray luminosities. The latter has been corrected for absorption using the hardness ratio reported in Fiore et al. (2001).

It is clear from Figures 4 and 5 that the radio-loud objects are associated mainly with Type 1 AGNs with  $L_{5-10 \text{ keV}} \gtrsim 10^{44} \text{ erg/s}$ , while all the Type 2 AGNs and Emis-

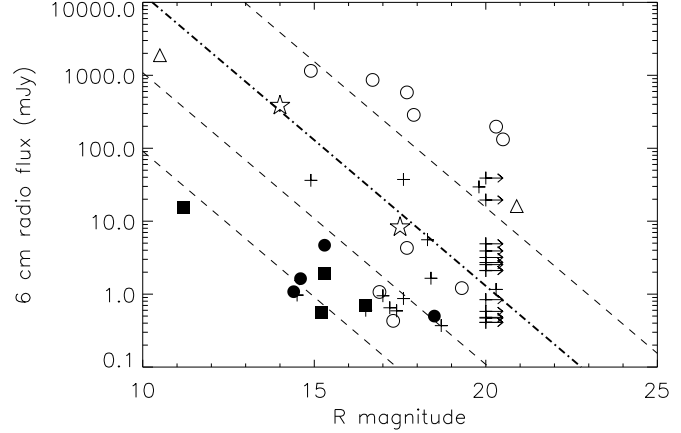


**Figure 4.** The R-band magnitude versus the 6 cm radio flux. Open circles : Type 1 AGN; filled circles : Type 2 AGN; Open Stars : BL LAC objects; Filled Squares : Emission Line Galaxies; Open Triangles : Radio Galaxies; Crosses : Unidentified HELLAS sources. The lines represent different two point spectral index  $\alpha_{ro}$ , corresponding to  $\alpha_{ro} = -0.05, 0.15, 0.35$  and  $0.55$  (from left to right). Objects above the dot dashed line ( $\alpha_{ro}=0.35$ ) are RL sources.

sion Line Galaxies are radio-quiet sources with  $\alpha_{ro} \lesssim 0.15$  and  $L_{5-10 \text{ keV}} \lesssim 10^{44} \text{ erg/s}$ .

The lack of low luminosity radio-loud sources is well explained by the dependence of the radio-loud fraction to the X-ray and optical luminosity. The fraction of the radio-loud AGN changes, in fact, from  $\sim 18\%$  at  $L_x \simeq 4 \times 10^{44} \text{ erg/s}$  to  $\sim 2\%$  at  $L_x \simeq 2 \times 10^{43} \text{ erg/s}$  in X-ray selected samples (Della Ceca et al. 1994) and from  $\sim 20\%-50\%$  at  $M_B \simeq -24.5$  to  $\sim 7\%-8\%$  at fainter absolute magnitude in optically selected samples (Padovani 1993, La Franca et al. 1994, Goldschmidt et al. 1999).

The lack of high X-ray luminosity Type 2 AGN is also a well known effect. Only few examples have been reported prior the *Chandra* mission (see, for example, Almaini et al. 1995, Boyle et al. 1998, Franceschini et al. 2000). However, even in the deeper *Chandra* and XMM surveys only a couple of sources considered as the prototype of Type 2 QSO ( $L_{2-10} > 10^{44}$ ,  $N_H > 10^{23} \text{ cm}^{-2}$ , optical emission lines with  $\text{FWHM} \lesssim 2000 \text{ km/s}$ ) have been detected (Norman et al. 2002, Stern et al. 2002). Their space density will be better constrained by the forthcoming deep X-ray (*Chandra* and XMM) and far-infrared surveys (SIRTF).

Finally, in Figure 6 we show the  $\alpha_{ox}-\alpha_{ro}$  plot for the 84 HELLAS sources for which we were able to calculate  $\alpha_{ox}$  and  $\alpha_{ro}$ . From this figure it is evident that the RQ Type 1 AGNs and the Type 2 AGNs occupy the same region in the plane  $\alpha_{ox}-\alpha_{ro}$  and then the two classes cannot be distinguished only on the basis of their multiband photometric data. On the other hand, the region with  $\alpha_{ox} \lesssim 1.5$  and  $\alpha_{ro} \gtrsim 0.35$  is occupied only by Type 1 AGN. We would therefore conclude that all the unidentified sources with  $\alpha_{ro} \gtrsim 0.30 - 0.35$  and  $\alpha_{ox} \lesssim 1.5$  are likely to be Type 1 AGN.

**Table 2.** Summary of the radio/X-ray associations from different X-ray surveys

X-RAY SURVEY	$f_x$ limit erg/sec/cm <sup>2</sup>	$f_r$ limit mJy	$f_r/f_{2keV}$ ( $\times 10^3$ )	% Radio/X associations
<sup>1</sup> Marano ROSAT + 20cm ATCA	$4 \times 10^{-15}$ (0.5-2.0 keV)	0.20	335	(4/50) $\sim$ 8%
<sup>2</sup> LOCKMAN ROSAT + 6cm VLA	$1 \times 10^{-15}$ (0.5-2.0 keV)	0.05	279	(8/54) $\sim$ 15%
<sup>3</sup> CRSS ROSAT + 20cm VLA	$2 \times 10^{-14}$ (0.5-2.0 keV)	0.70	234	(7/80) $\sim$ 9%
<sup>4</sup> EMSS <i>Einstein</i> + 6cm VLA	$8 \times 10^{-14}$ (0.3-3.5 keV)	0.80	119	(167/625) $\sim$ 27%
<sup>5</sup> LSS ASCA + 20cm FIRST	$1 \times 10^{-13}$ (2.0-10 keV)	1.00	78	(12/34) $\sim$ 35%
<sup>6</sup> HELLAS <i>BeppoSAX</i> + 6cm VLA-ATCA	$5 \times 10^{-14}$ (5.0-10 keV)	0.30	20	(53/147) $\sim$ 36%

<sup>1</sup> Zamorani et al. 1999; <sup>2</sup> Ciliegi et al. 2003; <sup>3</sup> Ciliegi et al. 1995; <sup>4</sup> Stocke et al. 1991; <sup>5</sup> Akiyama et al. 2000; <sup>6</sup> this work

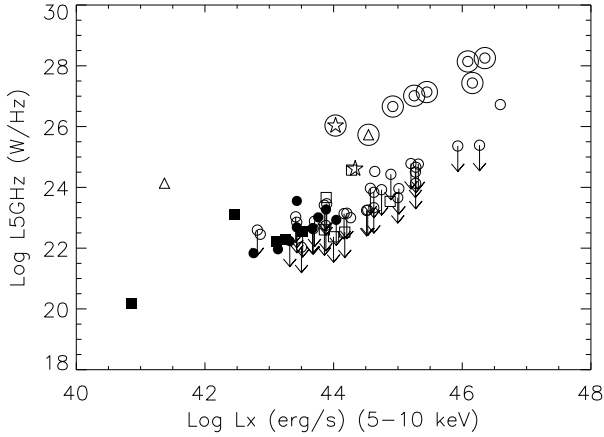


**Figure 5.** Radio versus hard X-ray luminosity for the HELLAS sample. The X-ray luminosity has been corrected for the photoelectric absorption. The sources with the encircled symbol are the objects classified as radio-loud sources on the basis of their radio to optical ratio  $\alpha_{ro} > 0.35$ . Symbols as in Figure 4. The six empty squares show the sources identified as cluster.

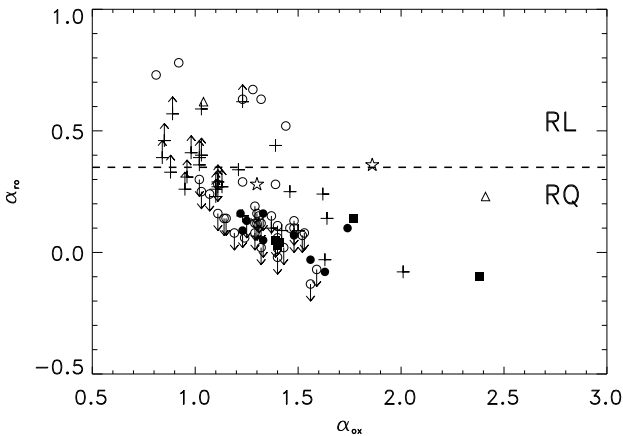


**Figure 6.** Overall energy distributions for the HELLAS sources. The axes are the radio-to-optical  $\alpha_{ro}$  and the X-ray-to-optical  $\alpha_{ox}$  two point spectral indices. The objects plotted are the 84 HELLAS sources for which we were able to calculate  $\alpha_{ox}$  and  $\alpha_{ro}$ . The horizontal dashed line shows the value of  $\alpha_{ro}=0.35$  used to divided RL and RQ objects. Symbols as in Figure 4.

## 4.2 Comparison with other X-ray samples

### 4.2.1 The *Einstein* Observatory, ROSAT and ASCA surveys

Previous radio follow-up of X-ray selected samples have shown different percentages of radio/X-ray associations. Using 20 cm observations of ROSAT X-ray selected sample, Ciliegi et al. (1995), de Ruiter et al. (1997) and Zamorani et al. (1999) found only  $\sim 10\%$  of radio/X-ray coincidences, while Stocke et al. (1991) found a significantly higher fraction (about 27%) for the X-ray sources in the *Einstein* Extended Medium Sensitivity Survey (EMSS). For the HELLAS sources we have 53 radio/X-ray associations over a total of 147 sources. From the statistical analysis of the radio/X-ray associations (see Section 3), we estimate that about 10% (*i.e.*  $\sim 5$  sources) of the proposed associations may be spurious and therefore the percentage with the “correct” radio/X-ray associations is in the range  $\sim 33\text{--}36\%$ . This value is comparable to that obtained by Akiyama et al. (2000) in the course of the ASCA Large Sky Survey ( $\sim 35\%$ ), one of the few large area samples selected in the hard X-ray band and with a complete follow-up in the radio and optical bands.

In Table 2 we report a summary of different X-ray surveys for which a complete radio follow-up is available. All these surveys are “AGN dominated” in the sense that the large majority of their identification ( $\geq 75\%$ ) are associated with AGNs. For each survey we report the X-ray and radio limits, the radio-to-X-ray limit ratio  $f_r/f_{2keV}$  assuming an X-ray spectral index  $\alpha_x=1.0$ , the percentage of radio/X associations (number of radio/X-ray association over the total number of X-ray sources in the survey) and the fraction of Radio-Loud objects in the radio/X-ray associations. As clearly shown in the table, the percentage of radio/X-ray associations is a function, as expected, of  $f_r/f_{2keV}$ : the lower this ratio is (*i.e.* deeper radio data in comparison to the X-ray flux limit) the higher is the fraction of X-ray objects with a radio counterpart. The top panel of Figure 3 suggests (as proposed also by Akiyama et al. 2000) that this change in the percentage of radio/X-ray associations is due to the fact that when  $f_r/f_{2keV}$  becomes very low we start seeing also radio-quiet AGNs. To check if this is the case, in Figure 7 we plot the 6 cm radio flux as function of the two point spectral index  $\alpha_{ro}$  for the HELLAS sources and for the 12 radio/X-ray associations found in the ASCA LSS (using a radio spectral index  $\alpha_r=0.7$  to convert the radio fluxes from 20 cm to 6 cm). The solid line shows the limit beyond which a source can not be detected in the optical band due to the magnitude limit of the optical data. The line in Figure 7 has



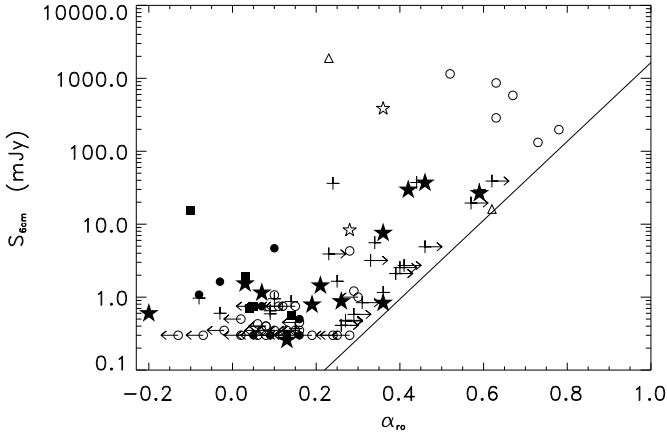


**Figure 7.** The 6 cm radio flux as function of the two point spectral index  $\alpha_{ro}$  for the HELLAS sources (symbols as in Figure 4) and for the 12 radio/X-ray associations found by Akiyama et al. (2000) in the ASCA LSS survey (filled stars). The solid line shows the limit beyond which a source can not be detected in the optical band due to the magnitude limit of the optical data ( $R=21$  mag).

been drawn using  $R=21$ . As clearly shown in figure, going deeper in the radio data we start to see the radio-quiet population ( $\alpha_{ro} < 0.35$ ). This population is almost completely absent at radio flux level greater than 10-20 mJy but becomes the dominant population at radio fluxes lower than  $\sim 1$  mJy. From Figure 7 it is also evident that deep optical data are needed in order to detect in the optical band radio-loud sources with radio fluxes lower than a few mJy.

Moreover it is interesting to note that the 3 X-ray surveys with the highest percentage of radio/X-ray associations (EMSS, LSS and HELLAS) are all selected in the medium or hard X-ray band (see Table 2), while the 3 X-ray surveys with the lowest percentage of radio/X-ray associations (Lockman, Marano and CRSS) are all selected in the soft X-ray band. In addition to the lowest radio-to-X-ray flux ratio available in the EMSS, LSS and HELLAS surveys, the higher percentage of radio/X-ray associations could also be due to the selection in the hard X-ray band. In fact, since the radio emission is transparent against obscuring material, obscured AGNs are detected in an unbiased way in the radio wavelength as well as in the hard X-ray band, but they could be missed in samples selected in the soft X-ray band where obscuration effects are much more relevant. To test this hypothesis we calculate the fraction of radio/X-ray associations in the HELLAS and LSS surveys using a radio flux limits of 3.7 mJy and 3.2 mJy respectively, in order to have an  $\text{fr}/f_{2\text{keV}}$  similar to that of the soft X-ray selected samples (see Table 2). We found a percentage of radio/X-ray associations around 20%, i.e. still higher than that found in soft X-ray selected samples. In conclusion the higher fraction of radio/X-ray associations found in the EMSS, LSS and HELLAS surveys in comparison to the soft X-ray selected samples is probably due to a combination of two effects: deeper radio data in comparison to the X-ray flux limit and the selection in harder X-ray bands.

#### 4.2.2 The deep Chandra surveys

Recently new deep X-ray samples have been obtained thanks to the revolutionary capabilities of the *Chandra* X-ray satellite. The deep surveys (Brandt et al. 2001, Rosati et al. 2002) have reached flux limits at least two orders of magnitude lower than the fainter samples listed in Table 2. Extensive programs of optical identifications showed that most of the sources in these samples are not AGN. The bulk of the optical identifications in these deep X-ray surveys is associated with normal galaxies, the majority of which show strong emission lines indicative of star formation activity (Barger et al. 2001, Brandt et al. 2001, Bauer et al. 2002). However, the most surprising finding is the discovery of a sizeable number of relatively bright X-ray sources spectroscopically identified with early-type “normal” galaxies without any signature of nuclear activity in the optical spectra (Fiore et al. 2000, Barger et al. 2001). These optically normal X-ray luminous galaxies were thought to be relatively rare, unusual objects, but during the recent deep X-ray surveys obtained with *Chandra* and XMM we saw a remarkable increase of their number (Comastri et al. 2002).

The radio properties of these new deep X-ray samples have been studied using very deep VLA radio survey (down to few micro Jy at 1.4 GHz) obtained in the SSA13 field (Barger et al. 2001) and in the HDF-N (Bauer et al. 2002). These studies showed a different behavior of these new samples in comparison to the “AGN-dominated” samples. In fact, in the new deep X-ray surveys a very high percentage of radio/X-ray associations (up to 80% in the SSA13 field, see Barger et al. 2001) has been found, with the highest matching fraction found among the emission line galaxies, which are comprised of apparently normal and starburst galaxies at redshift of  $z \sim 0.1-1.3$  thought to be undergoing recent star formation. The nature of the radio/X-ray associations is therefore completely different between that found in the “AGN dominated” samples reported in Table 2 and that found in the new deep X-ray surveys. While the former are associated with an AGN activity, the latter are mainly associated with a star forming activity.

#### 4.3 The radio spectral index

Using all the radio data available at 3, 6 and 20 cm we were able to calculate the radio spectral index (or an upper/lower limit when the source is detected in only one radio band) for a total of 50 HELLAS sources. Since the majority of the spectral indices have been calculated using the 6 cm fluxes obtained with our observations and the 20 cm fluxes reported in the public catalogues (NVSS and FIRST), their values should be treated as approximate since the images used to measure the fluxes were not matched in resolution. We also caution that variability among the radio AGN is a legitimate concern and could lead to inaccurate spectral index estimates since the two radio bands were observed several years apart.

All the radio spectral index  $\alpha_r$  are reported in column X of Table 1, while in Figure 8 we plot  $\alpha_r$  as function of the two point spectral index  $\alpha_{ro}$ . The horizontal dashed line denotes the typical spectral index,  $\alpha_r=0.5$ , separating steep and flat spectrum radio sources. Steep spectral indices ( $\alpha_r > 0.5$ ) often indicate radio emission from star formation

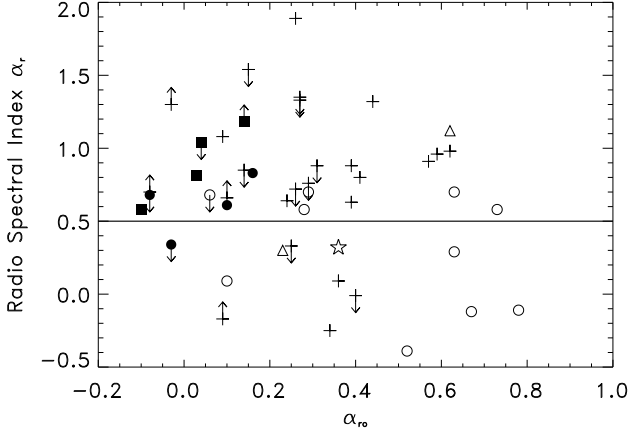


**Figure 8.** The radio spectral index as function of the two point spectral index  $\alpha_{ro}$  for the 50 HELLAS sources for which an information on the radio spectral index is available. Symbols as in Figure 4.

or lobe-dominated AGN, while flat ones ( $\alpha_r < 0.5$ ) often indicate emission from core-dominated AGN (e.g. Kellermann and Owen 1988).

A statistical analysis using both the measured values and the limits to  $\alpha_r$  has been performed with the software package ASURV, which implements the methods described by Feigelson & Nelson (1985) and Isobe, Feigelson & Nelson (1986). We divided our sources according to their optical classification studying the mean radio spectral index of sources with broad emission lines (AGN1, open circles in Figure 8) and with narrow emission lines (AGN2 plus Emission Line Galaxies, filled symbols in Figure 8). We found that while the Type 1 AGNs have a mean radio spectral index of  $\alpha_r = 0.25 \pm 0.10$ , the Type 2 AGNs plus the Emission Line Galaxies have a steeper radio spectral index  $\alpha_r = 0.69 \pm 0.11$ . This result is in agreement with the idea that the radio emission from Type 1 AGNs is core dominated with a flat radio spectral index due to the self-absorption process. On the other hand, in Type 2 AGN and Emission Line Galaxies the nonthermal radio emission (either due to a compact nucleus or to the integrated emission arising from the supernovae remnants in a starburst region) takes place on larger physical scale without self-absorption. For the case of the star formation these scales correspond approximately to 0.1-1.0 Kpc as observed in the local ELGs population (Condon 1989, Condon 1992) while for the core dominated sources these scales correspond to few parsec as well-known from many different radio surveys (see Nagar et al. 2000, 2002 and Giovannini et al. 2001 for the most recent works). Under this hypothesis, we expect a more extended radio emission from the HELLAS Type 2 AGNs and ELGs in comparison to the radio emission from the HELLAS Type 1 AGNs. Sub-arcsecond radio observations are needed to test this hypothesis.

#### 4.4 Radio Quiet and Radio Loud AGNs in the HELLAS spectroscopically identified subsample

Starting from the 61 spectroscopically identified sample of 118 HELLAS sources published by LF02 we selected a subsample of 46 AGNs (37 Type 1 + 9 Type 2) brighter than  $5 \times 10^{-14}$  erg cm $^{-2}$  s $^{-1}$  in the 5-10 keV band and brighter than R=21 and R=19 (for Type 1 and Type 2 AGNs) in the optical band. Radio data are available for all the 46 HELLAS AGNs. Using the two point spectral index  $\alpha_{ro}=0.35$  we divided the sources in RL and RQ. We have 6 ( $\sim 13\%$ ) RL sources, all classified as Type 1 AGN.

This fraction of RL AGNs is well in agreement with the predictions of Della Ceca et al. (1994). Using the de-evolved X-ray Luminosity function for RL and RQ AGNs they predicted a fraction of RL AGNs of  $\sim 10\%$  for an X-ray flux limit of  $\sim 5 \times 10^{-14}$  erg cm $^{-2}$  s $^{-1}$  (see their Figure 11).

## 5 SUMMARY AND CONCLUSION

We present the results of a complete radio follow-up down to a 6 cm flux limit of about 0.3 mJy (3  $\sigma$ ) obtained with the VLA and ATCA radio telescopes of all the 147 X-ray sources detected in the *BeppoSAX* HELLAS survey. Our major conclusions are as follows.

- From a statistical analysis based on the X-ray, optical and radio position, we found 53 X-ray/radio associations over a total of 147 sources. We estimated that about 10% (i.e.  $\sim 5$  sources) of the proposed associations may be spurious and therefore the percentage of the “real” X-ray/radio associations is in the range  $\sim 33-36\%$ . This percentage is in agreement to that obtained in other X-ray surveys selected in the hard X-ray band and is significantly greater than the percentage found in surveys selected in the soft X-ray band. This is probably due to a combination of two effects: the availability of deeper radio data in comparison to the X-ray flux limit and a selection in harder X-ray band. Obscured AGNs are in fact missed in soft X-ray selected samples, while they are detected in the radio and hard X-ray bands since both these wavelengths are transparent against obscuring material. This change in the percentage and nature of the radio/X-ray associations that we start to see in the HELLAS survey is much more evident in the new deep X-ray *Chandra* samples. Radio observations at the micro Jy level of the *Chandra* samples showed, in fact, that the radio/X-ray associations in these samples are dominated by normal galaxies and starburst at  $z \sim 0.1-1.3$ .

- The value of  $\alpha_{ro} = 0.35$  used to separate the radio-loud and radio-quiet sources has been estimated using the Lee statistic. Of the 53 HELLAS radio/X-ray associations, 26 have been classified as radio-loud sources. From the analysis of the ratio between the radio and the X-ray fluxes, we have assumed that all the 63 sources for which it was impossible to calculate the two point spectral index  $\alpha_{ro}$  (and than to obtain a classification in RQ or RL sources) are likely to be radio-quiet objects. Under this hypothesis, the fraction of radio-loud objects in the HELLAS sample is  $\sim 18$  per cent.

- The analysis of the multiband photometric data based on the two point spectral indices  $\alpha_{ro}$  and  $\alpha_{ox}$  has shown that the identified radio-loud objects are associated mainly with

Type 1 AGN with  $L_{5-10\text{ keV}} \gtrsim 10^{44}$  erg/s, while the identified Type 2 AGNs and Emission Line Galaxies are radio-quiet sources with  $L_{5-10\text{ keV}} \lesssim 10^{44}$  erg/s. RQ Type 1 AGNs and Type 2 AGNs cannot be distinguished only on the basis of their photometric data. On the basis of these results we would conclude that all the unidentified sources with  $\alpha_{ro} \gtrsim 0.30 - 0.35$  and  $\alpha_{ox} \lesssim 1.5$  are likely to be Type 1 AGN.

- The analysis of radio spectral index has shown that Type 1 AGNs have a mean spectral index flatter than Type 2 AGNs and Emission Line Galaxies. This result is in agreement with the idea that the core-dominated radio emission from Type 1 AGNs is self-absorbed, while in AGN2 and Emission Line Galaxies the radio emission take place on larger physical scale, without self-absorption.

- Finally, using a subsample of 46 AGNs (37 Type 1 and 9 Type 2, see section 4.4) we studied the fraction of the RL and RQ AGNs. We have 6 ( $\sim 13\%$ ) RL sources, all classified as Type 1 AGN. This fraction of RL AGNs is well in agreement with the results of Della Ceca et al. 1994 which predicted a fraction of RL AGNs of  $\sim 10\%$  for an X-ray flux limit of  $\sim 5 \times 10^{-14}$  erg cm $^{-2}$  s $^{-1}$ .

### Acknowledgements

This paper is based on observations collected at the Very Large Array (VLA) Radio Telescope and at the Australia Telescope Compact Array (ATCA). The VLA is a facility of National Radio Astronomy Observatory (NRAO) which is operated by Associated Universities, Inc., under cooperative agreement with the National Science Foundation. The ATCA is part of the Australia Telescope which is funded by the Commonwealth of Australia for operation as a National Facility managed by CSIRO. This work was supported by the Italian Ministry for University and Research (MURST) under grant COFIN-00-02-36 and by Italian Space Agency ASI contracts I/R/113/01 and I/R/073/01. CV also acknowledges the NASA LTSA grant NAG5-8107 for financial support.

### REFERENCES

- Akiyama M. et al. 2001, ApJ, 532, 700  
 Almaini O., Boyle B.J., Griffiths R.E., Shanks T., Stewart G.C., Georgantopoulos I., 1995, MNRAS, 277, L31  
 Barger A.J., Cowie L.L., Mushotzky R.F., Richards E.A., 2001, AJ, 121, 662  
 Bauer F.E., Alexander D.M., Brandt W.N., Hornschemeier A.E., Vignali C., Garmire G.P., Schneider D.P., 2002, AJ, 124, 2351  
 Boyle et al., 1998, MNRAS, 297, L53  
 Brandt W.N., et al. 2001, AJ, 122, 2810  
 Cilieggi P., Zamorani G., Hasinger G., Lehmann I., Szokoly G., Wilson G., 2003, A&A, 398, 901  
 Cilieggi P., Elvis M., Wilkes B.J., Boyle B.J., McMahon R.G., Maccacaro T., 1995, MNRAS, 277, 1463  
 Comastri A., Fiore F., Vignali C., Matt G., Perola G. C., La Franca F., 2001, MNRAS, 327, 781  
 Comastri A. et al. 2002, Proceeding of "New Visions of the X-ray Universe in the XMM-Newton and Chandra Era", 26-30 November 2001, ESTEC, The Netherlands, in press, astroph 0203019  
 Condon J.J., 1989, ApJ, 338, 13  
 Condon J.J., 1992, ARA&A, 30, 575  
 Condon J.J., Cotton W.D., Greisen E.W., Yin Q.F., Perley R.A., Taylor G.B., Broderick J.J., 1998, AJ, 115, 1693  
 de Ruiter H.R., Zamorani G., Parma P., Hasinger G., Hartner G., Trümper J., Burg R., Giacconi R., Schmidt M., 1997, A&A 319, 7  
 Della Ceca R., Zamorani G., Maccacaro T., Wolter A., Griffiths R., Stocke J.T., Setti G., 1994, ApJ, 430, 533.  
 Elvis M. et al., 1994, ApJSS, 95, 1.  
 Feigelson E.D., Nelson P.I., 1985, ApJ, 293, 192  
 Fiore F., et al. 2000, New Astronomy, 5, 143  
 Fiore F., Giommi P., Vignali C., Comastri A., Matt G., Perola G.C., La Franca F., Molendi S., Tamburelli F., Antonelli A., 2001, MNRAS, 327, 771  
 Fitchett M., Merrit D., 1988, ApJ, 335, 18  
 Fomalont E.B., Windhorst R.A., Kristian J.A., Kellerman K.I., 1991, AJ, 102, 1258.  
 Franceschini A., Bassani L., Cappi M., Granato G. L., Malaguti G., Palazzi, E., Persic M., 2000, A&A, 353, 910  
 Giommi P., Menna M. T., Padovani P., 1999, MNRAS, 310, 465  
 Giovannini G., Cotton W. D., Feretti L., Lara L., Venturi T., 2001, ApJ, 552, 508  
 Goldschmidt P., Kukula M.J., Miller L., Dunlop J.S., 1999, ApJ, 511, 612,  
 Isobe T., Feigelson E.D., Nelson P.I., 1986, ApJ, 306, 490  
 Kellermann K. I., Owen F. N., 1988, in Galactic and Extragalactic Radio Astronomy, eds G.L. Verschuur and K.I. Kellermann (New York: Springer)  
 La Franca F., Fiore D., Vignali C., Antonelli A., Comastri A., Giommi P., Matt G., Molendi S., Perola G.C., Pompilio F., 2002, ApJ, 570, 100  
 La Franca F., Gregorini L., Cristiani S., de Ruiter H., Owen F., 1994, AJ, 108, 1548  
 Lee K., 1979, J. Am. Statistical Assoc, 74, No, 367, 708  
 Lehmann I., Hasinger G., Schmidt M., Gunn J.E., Schneider D.P., Giacconi R., McCaughrean M., Trümper J., Zamorani G., 2000, A&A, 354, 35  
 Nagar N. M., Falcke H., Wilson A. S., Ulvestad, J. S., 2002, A&A, 392, 53  
 Nagar N. M., Falcke H., Wilson A. S., Ho L. C., 2000, ApJ, 542, 186  
 Norman C., et al. 2002, ApJ, 571, 218  
 Padovani P., 1993, MNRAS, 263, 461.  
 Rosati P., et al. 2002, ApJ, 566, 667  
 Schmidt M., Green R.F., 1983, ApJ, 269, 352  
 Stern D., et al. 2002, ApJ, 568, 71  
 Stocke J.T., Morris S.L., Gioia I.M., Maccacaro T., Schild R.E., Wolter A., Fleming T.A., Henry J.P., 1991, ApJS, 76, 813  
 Vignali C., Comastri A., Fiore, F., La Franca F., 2001, A&A, 370, 900  
 Vignali 2001, *The High Energy LLarge Area Survey (HELLAS): probing the multiwavelength properties of sources making the hard X-ray background*, PhD thesis, Bologna University, Italy.  
 White R.L., Becker R.H., Helfand D.J., Gregg M.D., 1997, ApJ, 475, 479  
 Zamorani G. et al., 1981, ApJ, 245, 357.  
 Zamorani G. et al. 1999, A&A, 346, 731